

# Europium location in the AIN: Eu green phosphor prepared by a gasreduction-nitridation route

Liang-Jun Yin, Qiang-Qiang Zhu, Wei Yu, Lu-Yuan Hao, Xin Xu et al.

Citation: J. Appl. Phys. 111, 053534 (2012); doi: 10.1063/1.3692810

View online: http://dx.doi.org/10.1063/1.3692810

View Table of Contents: http://jap.aip.org/resource/1/JAPIAU/v111/i5

Published by the American Institute of Physics.

## **Related Articles**

Modeling of carrier lifetimes in uniaxially strained GaAs J. Appl. Phys. 111, 103704 (2012)

Observation of band alignment transition in InAs/GaAsSb quantum dots by photoluminescence J. Appl. Phys. 111, 104302 (2012)

The role of glass-viscosity on the growth of semiconductor quantum dots in glass matrices J. Appl. Phys. 111, 094315 (2012)

Excitation-dependent recombination and diffusion near an isolated dislocation in GaAs J. Appl. Phys. 111, 093712 (2012)

Eu luminescence center created by Mg codoping in Eu-doped GaN Appl. Phys. Lett. 100, 171904 (2012)

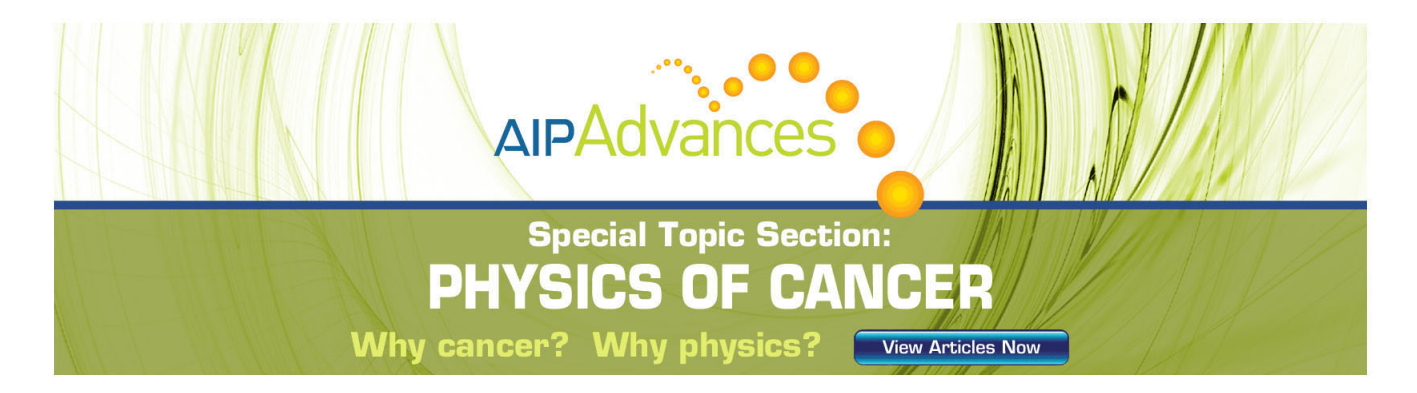
# Additional information on J. Appl. Phys.

Journal Homepage: http://jap.aip.org/

Journal Information: http://jap.aip.org/about/about\_the\_journal Top downloads: http://jap.aip.org/features/most\_downloaded

Information for Authors: http://jap.aip.org/authors

# ADVERTISEMENT



# Europium location in the AIN: Eu green phosphor prepared by a gas-reduction-nitridation route

Liang-Jun Yin, <sup>1</sup> Qiang-Qiang Zhu, <sup>1</sup> Wei Yu, <sup>1</sup> Lu-Yuan Hao, <sup>1</sup> Xin Xu, <sup>1,a)</sup> Feng-Chun Hu, <sup>2</sup> and Ming-Hsien Lee<sup>3</sup>

<sup>1</sup>Laboratory of Materials for Energy Conversion, Department of Materials Science and Engineering, University of Science and Technology of China, Hefei 230026, China

(Received 6 December 2011; accepted 10 February 2012; published online 15 March 2012)

Eu doped aluminum nitride phosphors were successfully synthesized by a novel gas-reduction-nitridation route with a reaction temperature of 1400 °C and a soaking time of 3 h. The obtained AlN:Eu phosphors were analyzed to elucidate the location of the Eu luminescent center. High-resolution transmission electron microscopy and transmission electron microscopy-energy dispersive spectra proved that Eu was located in the crystal lattice of AlN, then EXAFS revealed that Eu occupied a highly distorted Al site coordinated by four nitrogen at about 2.30–2.40 Å, and the second nearest neighbors of Eu were 12 Al. This could be confirmed by the first-principles calculations based on the obtained local structure around the Eu luminescence center, where the theoretical absorption spectrum was similar to the experimental excitation spectrum. X-ray appearance near edge structure showed that Eu existed in terms of both Eu<sup>3+</sup> and Eu<sup>2+</sup> ions, which could be related to the limited location space of Eu. High temperature treatment could significantly increase the amount of Eu<sup>2+</sup> by the expansion of the crystal lattice, leading to an increased green luminescence of the obtained AlN:Eu phosphors. © 2012 American Institute of Physics. [http://dx.doi.org/10.1063/1.3692810]

#### I. INTRODUCTION

Nowadays, light-emitting-diodes (LEDs) show high potential for replacement of conventional lighting sources due to many advantages, such as long lifetime, low energy consumption, high reliability, and environmental-friendly affiliation. <sup>1,2</sup> One of the key factors for governing the device performance is the phosphors for light conversion. Much attention has been paid to the newly developed (oxy)nitride phosphors for the following two reasons. <sup>3–5</sup> First, strong covalent bonding between the luminescent center and the nitrogen lowers the energy of excitation state and gives a long emission wavelength, and the emission can be adjusted to a large extent from blue to red. Second, the high stabilities of nitride compounds make the phosphors appropriate for high-power and long life-time LED devices.

Aluminum nitride (AIN) has been widely studied for electronic packing applications owing to its high electrical insulation, high thermal conductivity, low thermal expansion coefficient, and high chemical stability.<sup>6,7</sup> It is also regarded as a potential candidate for photoluminescence and electroluminescence devices due to its wide bandgap (6.2 eV).<sup>8</sup> Many groups have reported rare-earth or transition metal doped AlN but most of them focused on thin films, <sup>9-14</sup> very few studies investigated powder phosphors. Although the luminescent properties of rare-earth doped AlN films have been extensively studied, it is still not clear where these luminescent ions locate in the wurtzite AlN lattice as there is not enough space for a large cation to occupy the tetrahedral Al sites.

Recently, Hirosaki et al. have prepared a blue Eu, Si codoped AlN phosphor with excellent luminescent properties and thermal stability to be used in white light-emitting diodes (LEDs) and field emission displays (FEDs) by a gas pressure sintering method at 2050 °C for 4 h under 10 atm N<sub>2</sub> pressure. 15,16 Later, they pointed out that Eu did not enter the crystal lattice of AlN, but Eu, Si formed a new layered structure in the grain boundary of AlN phase and Si codoping was essential for the Eu incorporation into AlN. 17 In our previous study, we obtained pure AIN phase with sole Eu doping by carbothermal reduction (CR) and showed detailed information about phase composition and luminescent properties.<sup>18</sup> The emission of AlN:Eu phosphor could be tuned widely from blue to green, depending on oxygen content in AlN matrix. Later, the effects of different fluxes on preparing AlN:Eu phosphor were investigated and it was found BaF2 flux can largely improve its luminescence intensity. 19 However, the exact location of Eu in the AlN crystal lattice is still unknown.

Although AlN:Eu phosphors produced by carbothermal reduction have the advantages of simplicity and relatively low cost, the residual carbon decreases luminescence intensity. Therefore, it is necessary to develop an alternative method in order to obtain phosphors without residual carbon. Suehiro *et al.*<sup>20</sup> have synthesized pure AlN powders by gasreduction-nitridation (GRN) method using NH<sub>3</sub> and C<sub>3</sub>H<sub>8</sub> as reactant gases at a mild reaction temperature of 1300 °C for 1 h. The same group also succeeded in synthesizing the yellow-emitting Ca-a-SiAlON:Eu phosphor with good photoluminescence by this method.<sup>21</sup> In the present paper, the gas-reduction-nitridation synthesis of the AlN:Eu phosphors

<sup>&</sup>lt;sup>2</sup>National Synchrotron Radiation Laboratory, University of Science and Technology of China, Hefei, Hefei 230026, China

<sup>&</sup>lt;sup>3</sup>Department of Physics, Tamkang University, Tamsui, Taipei 251, Taiwan

a) Author to whom correspondence should be addressed. Electronic mail: xuxin@ustc.edu.cn.

was successfully performed, then the location of Eu in the AlN crystal lattice was studied in detail by high-resolution transmission electron microscopy-energy dispersive spectra (HRTEM-EDS) and EXAFS. This is very important to improve the luminescence properties and obtain some inspiration for AlN based phosphors doped with other large ions.

#### II. EXPERIMENTAL PROCEDURES

#### A. Synthesis

Powders with a composition of AlN:0.5 mol. % Eu were prepared by gas-reduction-nitridation method. The powder mixture of nano-sized  $\gamma$ -Al<sub>2</sub>O<sub>3</sub> (99.99 wt. %, 10 nm, specific surface area of 350 m<sup>2</sup>/g, Wanjing New Materials Co. Ltd), Eu<sub>2</sub>O<sub>3</sub> (99.99 wt. %, Sinopharm Chemical Reagent Co. Ltd) was well mixed in a Si<sub>3</sub>N<sub>4</sub> mortar by hand. The mixtures were put into BN crucibles and set in a horizontal alumina tube furnace. The samples were heated to 1200 °C at a heating rate of 5 °C/min, and then heated to the experimental reaction temperature of 1400 °C under a flowing gas mixture of 1 ml/min NH<sub>3</sub> and 15 ml/min CH<sub>4</sub>. After the predetermined holding time, the samples were cooled down naturally. CH<sub>4</sub> gas was shut off and only NH<sub>3</sub> gas was left with the flow rate of 0.3 l/min when the temperature reached 1200 °C. The products were post-annealed at 1800-2100 °C for 2 h in a carbon furnace under flowing nitrogen gas.

### **B.** Characterization

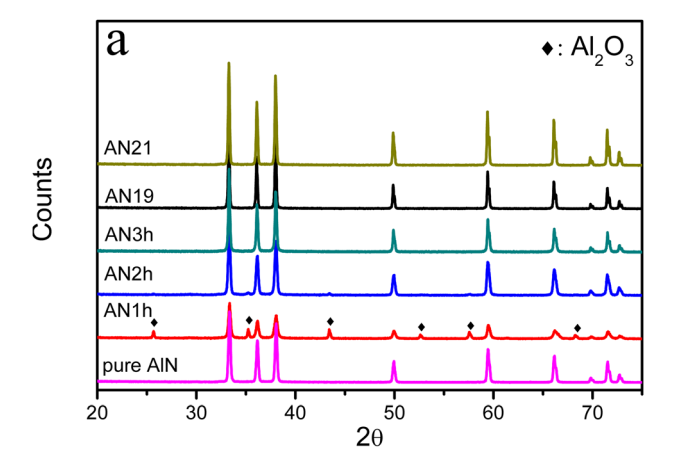
The phase was analyzed by an x-ray diffractometer (Model PW 1700, Philips Research Laboratories, Eindhoven, the Netherlands) using Cu K $\alpha$  radiation at a scanning rate of 0.5 °/min. The oxygen content was determined using a Nitrogen/Oxygen Analyzer (Model TC-436, LECO, Tokyo, Japan.). The inner structure was observed by transmission electron microscopy—energy dispersion x-ray spectroscopy (model 2100 F, JEOL, Tokyo, Japan). The x-ray absorption spectra at the Eu L<sub>3</sub>-edge were measured at the beamline of BL14W1 at Shanghai Synchrotron Radiation Facility. Finally, we used IFEFFIT-1.2.11 software package to analyze the results of the EXAFS data by standard methods.

#### C. Luminescence Properties

The photoluminescence spectra were measured at room temperature by a fluorescent spectrophotometer (Model F-4600, Hitachi, Tokyo, Japan) with a 200 W Xe lamp as an excitation source. The emission spectrum was corrected for the spectral response of the monochromator and Hamamatsu R928P photomultiplier tube (Hamamatsu Photonics K.K., Hamamatsu, Japan) by a light diffuser and tungsten lamp (Noma Electric Corp., New York; 10 V, 4 A). The excitation spectrum was also corrected for the spectral distribution of the xenon lamp intensity by measuring Rhodamine-B as reference.

# III. RESULTS AND DISCUSSION

Figure 1 shows the XRD patterns of the products prepared under different synthesis conditions. The powder fired



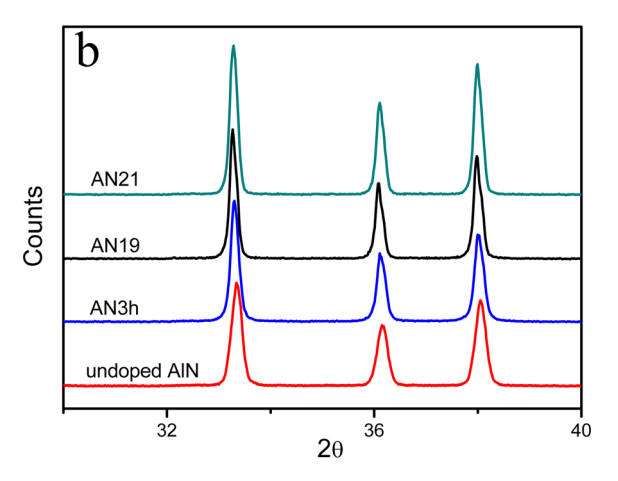


FIG. 1. (Color online) (a) The XRD patterns of undoped AlN, Eu doped AlN prepared at 1400  $^{\circ}$ C for 1–3 h (represented by AN1h, AN2h, and AN3h, respectively), and sample AN3h after post-annealing at 1900  $^{\circ}$ C and 2100  $^{\circ}$ C for 2 h in N<sub>2</sub> atmosphere (represented by AN19 and AN21, respectively). (b) The magnified XRD regions between 30–40 $^{\circ}$  of Fig. 1(a).

at 1400  $^{\circ}$ C for 1 h (AN1h) consists of AlN and unreacted Al<sub>2</sub>O<sub>3</sub> phase. The amount of AlN gradually increases with increasing holding time. Pure AlN phase is obtained without detectable Al<sub>2</sub>O<sub>3</sub> phase in the samples fired at 1400  $^{\circ}$ C for 3 h (AN3h). High temperature thermal treatments have little influence on the phase composition.

Table I shows the oxygen content and residual carbon of AlN:Eu phosphors prepared by GRN. For comparison, the results of AlN:Eu phosphors prepared by CR and solid-state reaction (SSR) are also presented. We selected a CR sample with the best luminescence properties, as reported before. Much lower carbon content is obtained in the phosphors synthesized by GRN. The phosphors synthesized by GRN are white, whereas the phosphors synthesized by CR are slight-gray.

TABLE I. Comparison of oxygen content and residual carbon in the powders synthesized by SSR, GRN, and CR respectively.

Samples	Oxygen content (wt. %)	Residual carbon (wt. %)
AN3h	1.31	0.021
AN21	0.61	0.006
AlN:Eu by CR	2.02	0.981
AlN:Eu by SSR	5.16	_

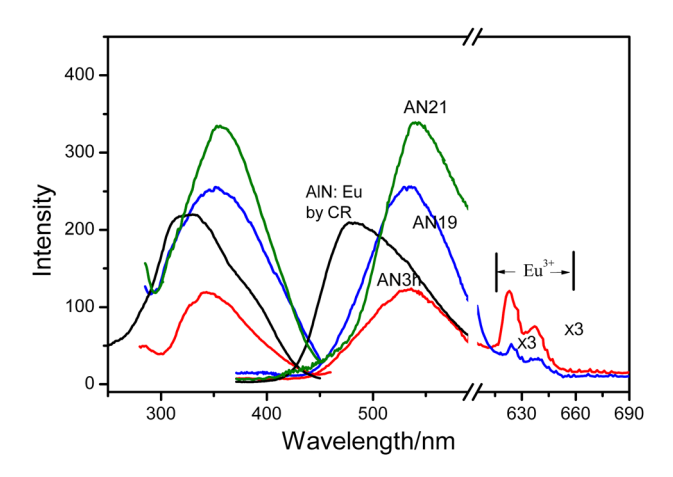


FIG. 2. (Color online) Photoluminescence spectra of AlN:Eu by CR and GRN.

AlN:Eu powders by SSR are formed at 1900 °C for 2 h in N<sub>2</sub> atmosphere, however, Eu could not enter the AlN crystal lattice, which is in good agreement with the previous report. The reason could be attributed to the different oxygen content. As shown in Table I, AlN:Eu phosphor synthesized by SSR shows much higher oxygen content than that synthesized by GRN and CR. So it is speculated that Eu preferably resides as a Eu rich impurity phase in AlN samples with high oxygen content.

As seen in Fig. 1(b), the diffraction peaks of Eu doped AlN phosphors slightly shift to lower angles, indicating the undoubted dissolution of Eu into AlN crystal structure. On the basis of calculations by UNITCELL software (the same software was used for other calculations in this paper.), the lattice parameters increase with the incorporation of Eu from a = 3.1065 Å, c = 4.9710 Å (undoped AIN) to a = 3.1076Å, c = 4.9733 Å (AN3 h). It appears that the larger Eu ions occupy Al sites, although there exists great difference of ionic radius between  $\mathrm{Eu}^{2+}$  (1.12 Å) and  $\mathrm{Al}^{3+}$  (0.50 Å). For AlN:Eu, Si phosphors reported before, the lattice parameters decreased with the incorporation of Eu, Si into AlN crystal lattice, probably due to the substitution of a smaller amount of Si into the AlN lattice.<sup>22</sup> So the surrounding environments of Eu in AlN:Eu phosphors differ from those in AlN:Eu, Si phosphors.

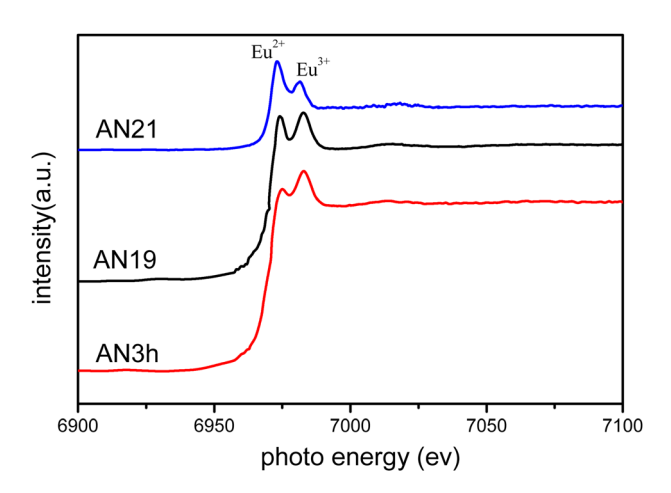
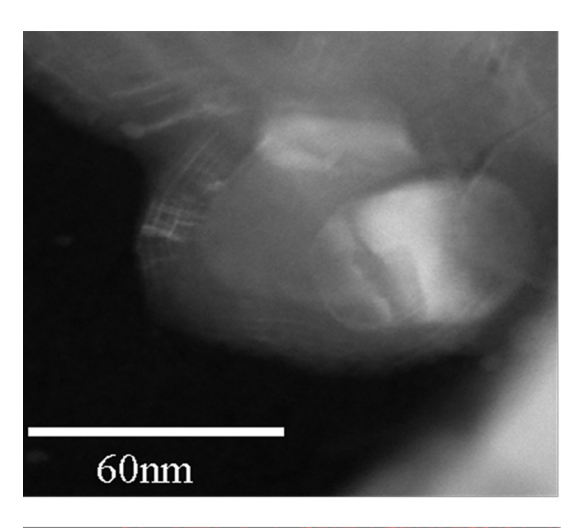
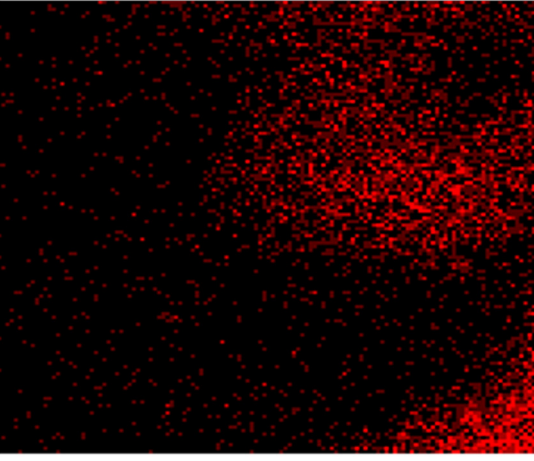


FIG. 3. (Color online) Normalized Eu  $L_{\rm III}\text{-}\text{edge}$  XANES of AN3h, AN19, and AN21 phosphors.

Figure 2 shows the photoluminescence spectra of AlN:Eu phosphors prepared by CR and GRN. GRN phosphors show broad green emission band at about 540 nm under 330 nm excitation, which is obviously ascribed to the 5d–4f transition of Eu<sup>2+</sup>. Compared with the 477 nm emission of CR phosphor, the emission spectra of GRN phosphors show a characteristic of redshift, which is due to their low oxygen content, as seen in Table I. The Eu<sup>2+</sup> luminescence greatly depends on the local coordination environments. The emissions of GRN





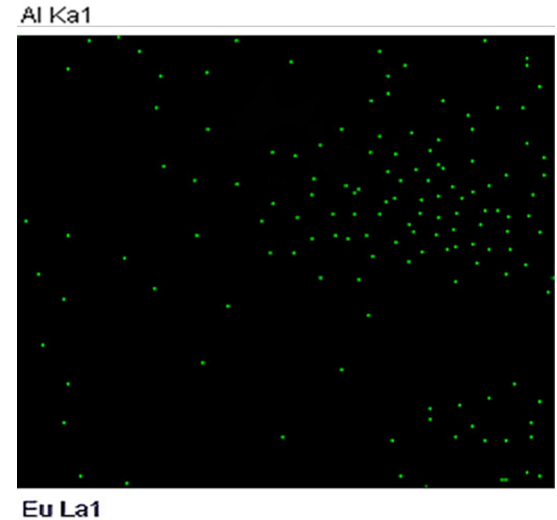


FIG. 4. (Color online) EDS maps showing the distribution of Al and Eu in AN21 phosphor.

AlN:Eu phosphors occur at longer wavelength, which is attributable to the higher formal charge of  $N^{3-}$  compared with  $O^{2-}$  and the lower electronegativity of nitrogen (3.04) compared with oxygen (3.44), called the nephelauxetic effect, which results in stronger crystal-field splitting and lower energy of the center of gravity of the 5d energy levels.<sup>23,24</sup>

It should be noted that sharp lines assigned to  $\mathrm{Eu}^{3+}$  intra-4f<sup>6</sup> transitions have been detected, indicating that there are  $\mathrm{Eu}^{3+}$  ions in the crystal lattice. Figure 3 shows the normalized Eu L<sub>III</sub>-edge XANES of AN3h, AN19, and AN21 phosphors. Two peaks can be clearly seen, at about 6977 and 6984 eV, which are due to the divalent and trivalent oxidation states of Eu, respectively. <sup>25</sup> Obviously, there are large amount of  $\mathrm{Eu}^{3+}$  ions accompanying  $\mathrm{Eu}^{2+}$  ions. The coexistence of  $\mathrm{Eu}^{2+}$  and  $\mathrm{Eu}^{3+}$ ,  $\mathrm{Mn}^{2+}$  and  $\mathrm{Mn}^{3+}$  is also identified in the Eu doped polycrystalline c-BN specimens and Mn doped AlN films, respectively. <sup>26,27</sup> A previous report showed that all Eu are divalent in Eu, Si-codoped AlN phosphors, <sup>17</sup> indicating that the surrounding environments of Eu in AlN:Eu phosphors differ from those in AlN:Eu, Si phosphors.

The Eu<sup>2+</sup>-to-Eu<sup>3+</sup> ratio can be significantly increased by post-annealing (1900–2100 °C), which leads to a luminescence increase in 540 nm emission and a luminescence decrease in 620 nm, as shown in Fig. 2. The luminescence assigned to Eu<sup>3+</sup> completely disappears in AN21 phosphor.

TEM-EDS mapping analyses are performed to study the chemical element distribution, as shown in Fig. 4. By comparing the EDS-mapping and the TEM of AlN:Eu particles, it is clearly seen that Eu concentrates in AlN particles. In order to clarify the local environment of Eu in AlN lattice, the HRTEM and electron diffraction image (ED) measurements of the same particle are shown in Fig. 5. For comparison, the images of the undoped AlN reference sample Figs. 5(c) and 5(d) are also

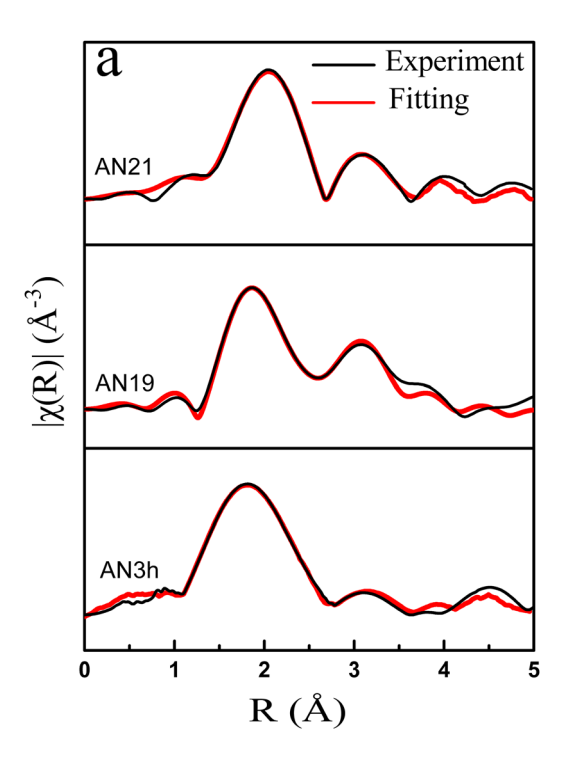


FIG. 6. (Color online) The Fourier transform of the Eu-L<sub>III</sub>-edge EXAFS spectrum. The experimental curve and the fitting are shown in black and red lines, respectively.

shown. In the electron diffraction image of AlN:Eu particle (Fig. 5(b)), there are some streaks but without apparent superlattice points, indicating that the long-range order has been lost. This is probably caused by the large lattice deformation due to the dissolution of large Eu ions in the AlN lattice.

To identify the exact location of Eu in the AlN structure, Eu  $L_{\rm III}$  edge EXAFS analysis is performed. Fourier

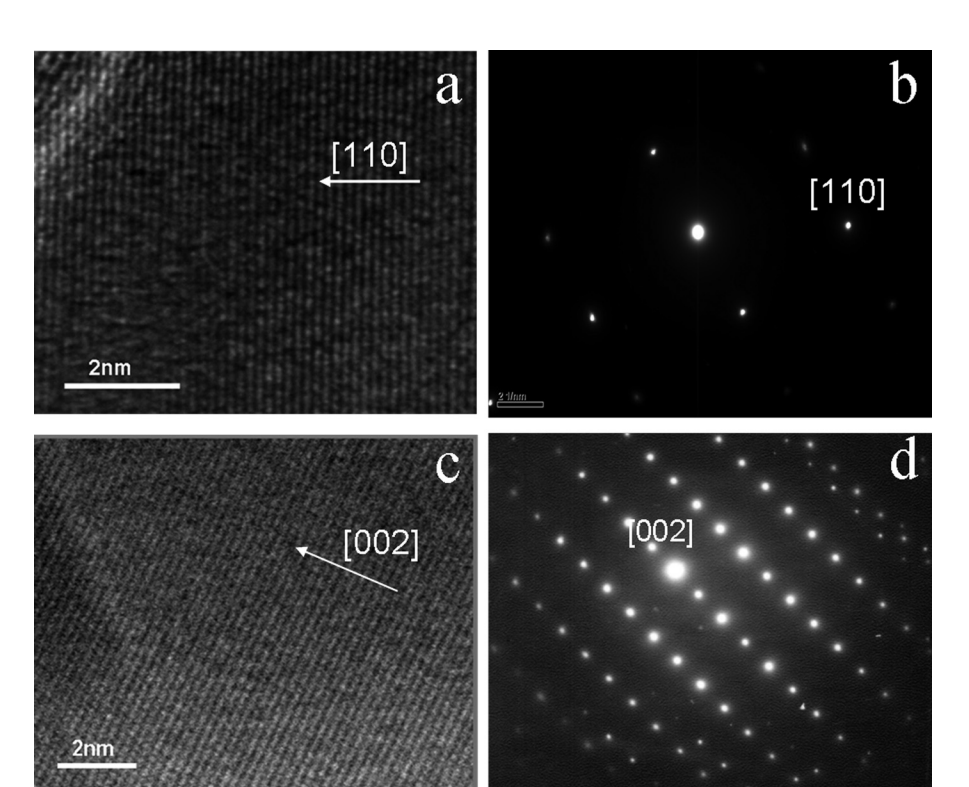


FIG. 5. TEM image (a) and ED picture (b) of the AN21 phosphor. The reference TEM image (c) and ED picture (d) for the undoped AlN are also shown as a comparison.

TABLE II. Analytical results of EXAFS from Eu-doped AlN.

Sample	Parameter	1st neighbor atoms		2nd neighbor atoms	
AN3h		1	N	Al	
	C.N.	3	<u>1</u>	<u>6</u>	6
	R (Å)	$2.28 \pm 0.06$	$2.31 \pm 0.06$	$3.10 \pm 0.21$	$3.14 \pm 0.21$
	$\delta^2  (\mathring{A}^2)$	$0.015 \pm 0.004$		$0.019 \pm 0.020$	
AN19		N		Al	
	C.N.	3	1	6	<u>6</u>
	R (Å)	$2.30 \pm 0.06$	$2.33 \pm 0.06$	$3.13 \pm 0.21$	$3.18 \pm 0.21$
	$\delta^2  (\mathring{A}^2)$	$0.019 \pm 0.009$		$0.022 \pm 0.011$	
AN21		N		Al	
	C.N.	3	1	6	<u>6</u>
	R (Å)	$2.40 \pm 0.04$	$2.44 \pm 0.04$	$3.18 \pm 0.17$	$3.22 \pm 0.17$
	$\delta^2  (\mathring{A}^2)$	$0.020 \pm 0.006$		$0.022 \pm 0.019$	

transformed data of three samples are shown in Fig. 6. Two main peaks are present in all the samples. For each edge, the first peak is attributed to the nearest N atoms and the second one is due to the nearest Al atoms. It is obvious that the Fourier transformed functions of these three samples are similar to one another, which indicates that they have similar local structures. The analyzed results are presented in Table II, which shows that Eu is coordinated by four N atoms, with second nearest neighbors of 12 Al. The Eu atoms are coordinated by four nitrogen atoms with two different bond lengths. For example, in the case of AN19, the obtained distances are 2.30 Å between Eu and three N atoms and 2.33 Å between Eu and another N atom. As shown in Fig. 7(a), the first and second nearest neighbor atoms of Al in AlN matrix are four N atoms and 12 Al atoms, in which the distances are 1.885 Å between Al and three N atoms and 1.917 Å between Al and another N atom,. The above results indicate the substitution of Eu in Al sites. The larger bond lengths in AlN:Eu phosphors than those in pure AIN powders are due to the larger radius of Eu ions. The  $\delta$ , a measure of local disorder, is extremely large. This result shows that the drastic structural change around Eu and the structural disorder become larger with the increase of  $Eu^{2+}$  ratio after post-annealing, because the radius of  $Eu^{2+}$  ion is larger than that of  $Eu^{3+}$ ion. This is in good accordance with the electron diffraction (ED) result (Fig. 5(b)).

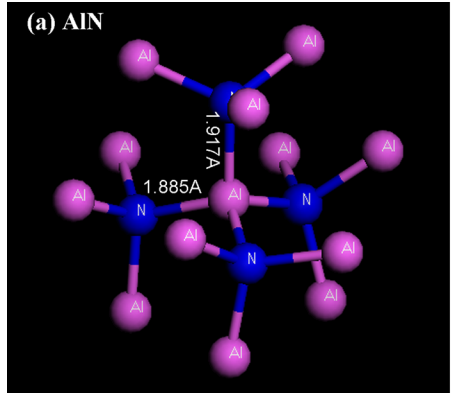
In fact, there are many reports on rare-earth or transition metal doping AlN films. Lattice location studies performed on AlN:Yb<sup>3+</sup> showed that Yb<sup>3+</sup> ions occupied substitutional

Al lattice sites. <sup>10</sup> XAFS measurements performed on AlN:  $\rm Mn^{2+}$  indicated that Mn ions occupied the Al lattice sites of AlN. <sup>27</sup> Ronning *et al.* also reported that In and Sr atoms mainly occupy substitutional lattice sites directly, according to the results of emission channeling (EC) and perturbed  $\gamma\gamma$  angular correlation (PAC). <sup>28</sup> So it is reasonable that Eu ions similarly occupy Al sites in AlN:Eu phosphors because Eu has a relatively smaller ionic radius [ $\rm r(Eu^{2+}) = 1.12~ \AA$ ,  $\rm r(Eu^{3+}) = 0.95~ \AA$ ,  $\rm r(In^+) = 1.32~ \AA$ ,  $\rm r(Sr^{2+}) = 1.13~ Å$ ]. Mares *et al.* speculated that Eu<sup>2+</sup> ions can replace Al<sup>3+</sup> in AlN lattice ( $\rm r^{cov}_{Al^{3+}} = 1.26~ Å$ ), but did not give detailed information. <sup>29</sup> Here, the authors make clear the Eu location in the AlN lattice and prove that Eu occupies Al sites by EDS-mapping, ED, and XAFS measurements.

Generally, Eu is divalent in the pure nitride phosphors prepared at high temperature due to the relatively lower electronegativity of N compared with that of O.<sup>3,30</sup> But in AlN:Eu phosphors prepared by GRN, Eu<sup>2+</sup> and Eu<sup>3+</sup> coexist. As shown in Fig. 3, the Eu<sup>3+</sup> content is significantly highly than the Eu<sup>2+</sup> content in the AN3h phosphor. This could be partly explained by the location of Eu. There is not enough space for the transition of Eu<sup>3+</sup> to Eu<sup>2+</sup>, because the radius of Eu<sup>2+</sup> is much higher than that of Eu<sup>3+</sup>. High temperature treatment could expand the crystal lattice, and promote the transition of Eu<sup>3+</sup> to Eu<sup>2+</sup>. High temperature treatment could expand the crystal lattice, and promote the transition of Eu<sup>3+</sup> to Eu<sup>2+</sup>. High temperature treatment could expand the crystal lattice, and promote the transition of Eu<sup>3+</sup> to Eu<sup>2+</sup>. High temperature treatment could expand the crystal lattice, and promote the transition of Eu<sup>3+</sup> to Eu<sup>2+</sup>.

In order to further clarify the Eu site and the origin of the absorption band, we perform first-principles calculations of optical absorption spectra of AlN:Eu and investigate the site of the Eu ions by comparing the theoretical absorption spectra with the experimental excitation spectra. According to the crystallographic data of AlN and EXAFS measurements of AN21, we construct a Eu cluster  $[\text{EuAl}_{12}\text{N}_4]^{26+}$ . In this structure, Eu ions replace some of the Al ions in AlN as central ions, each of which is surrounded by 4 nearestneighbor N ions, and 12 next nearest neighbor Al ions, as shown in Fig. 7(b).

For this cluster, the absorption spectrum and the density of states (DOS) calculations were performed using the CASTEP code.  $^{33-35}$  A plane wave basis set with kinetic energy cutoff at 500 eV was employed, and the Perdew-Burke-Enzerhof form  $^{36-38}$  of the generalized gradient approximation (GGA) was used to describe the exchange-correlation interactions, while the electron-ion interaction was accounted for through the use of ultrasoft pseudopotentials. The detailed parameters were chosen as follows: k-point spacing = 0.057  $\text{Å}^{-1}$ , sets of



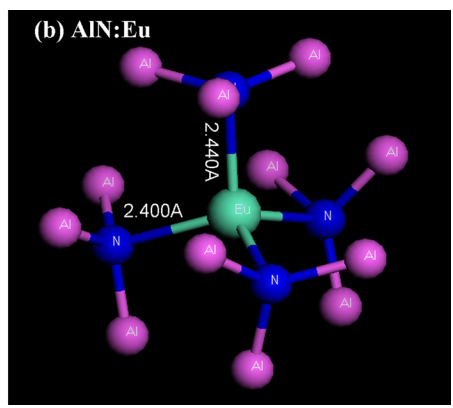


FIG. 7. (Color online) The structure of AlN (a) and AN21 (b).

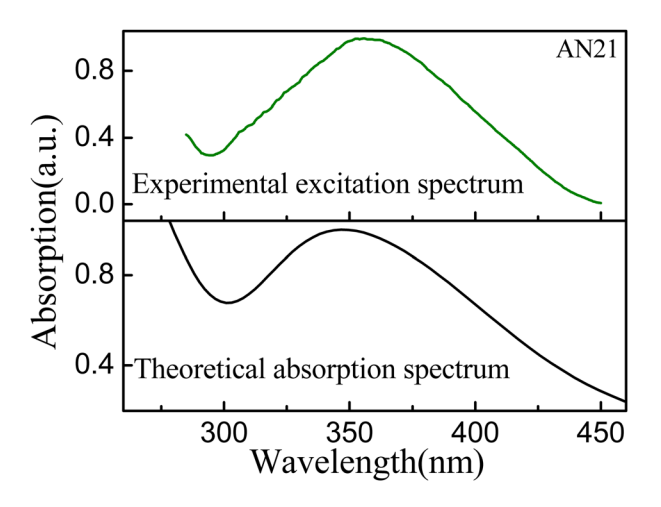


FIG. 8. (Color online) The experimental excitation spectrum and theoretical absorption spectrum.

k points =  $1 \times 1 \times 1$ , space representation = reciprocal, and SCF tolerance threshold =  $1.0 \times 10^{-6}$  eV/atom.

Figure 8 presents the calculated theoretical absorption spectrum from the  $\left[\text{EuAl}_{12}\text{N}_4\right]^{26+}$  cluster with CASTEP code. The experimental excitation spectrum for the sample AN21 is also shown for comparison. It is clear that the theoretical results are in good qualitative agreement with the experimental observations, which could support our conclusion about the location of Eu in the AlN structure.

Figure 9 shows the total and the atom-resolved partial DOS (PDOS) for all the different atoms in the constructed cluster. For clarity, the Fermi level is set to zero. Clearly, a sharp peak I around the Femi level mainly comes from Eu 4f states. The peak II around 3.5 eV is mostly contributed by Eu 5d and Eu 6p states with mixings of Al 4s and 4p states. By comparing Fig. 8 with Fig. 9, the experimental absorption peak around 350 nm (3.5 eV) clearly originates from the Eu  $4f^7 \rightarrow$  Eu 5d and 6p and Al 4s and 4p interband transitions. Eu ions are really responsible for the excitation spectrum.

The obtained AIN:Eu phosphors show a single intense broad green emission band, which is attributable to the allowed 4f<sup>6</sup>5d-4f<sup>7</sup> transition of Eu<sup>2+</sup>. Based on the crystal field theory, the 5d orbitals of Eu<sup>2+</sup> are split in the crystal field. This splitting is affected by the type of ligands, the arrangement of the ligands around the Eu<sup>2+</sup>, and the coordination distance between the Eu<sup>2+</sup> and the ligands. The higher formal charge of N<sup>3-</sup> compared with O<sup>2-</sup> and the lower electronegativity of nitrogen (3.04) compared with oxygen (3.44) often lead to larger ligand-field splitting of the 5d levels and the center of gravity of the 5d states at lower energy, resulting in a long emission wavelength. For some Eu<sup>2+</sup> doped pure nitride phosphors with proper ligand arrangement and short coordination distance, the emission peaks are situated in the red region, such as 610 nm for Eu doped SrAlSiN<sub>3</sub>(Sr-N:  $\sim$  2.7 Å, C.N. = 10) and 640 nm for Eu doped Sr<sub>2</sub>Si<sub>5</sub>N<sub>8</sub> (Sr-N:  $\sim 2.8$  Å, C.N. = 8–9). However, short-wavelength emission is also possible in the sample of weak crystal field, such as Eu doped  $SrSi_6N_8$  (C.N. = 10) and  $BaSi_7N_{10}$  (C.N. = 12) blue phosphor. 40,41 In these phosphors, large metal-ligand distances (>3 Å) and too high coordination number result in a weaker crystal-field splitting. In the AlN:Eu phosphors reported

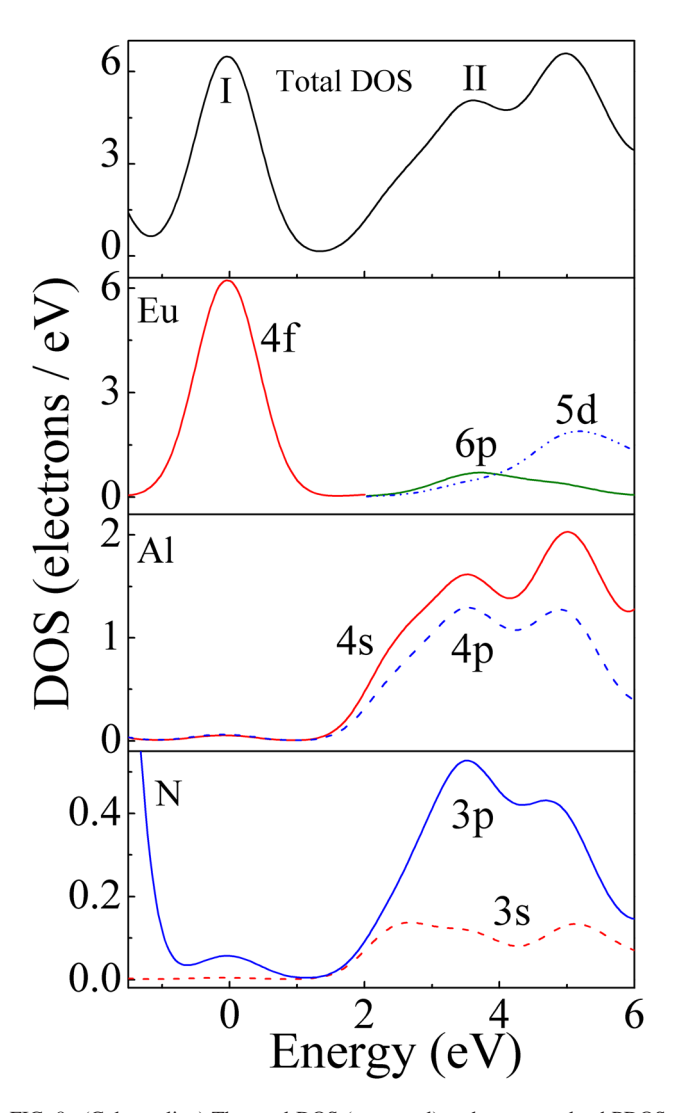


FIG. 9. (Color online) The total DOS (top panel) and atom-resolved PDOS in AlN:Eu.

here, although the coordination distance is as low as 2.3–2.4 Å, the weak tetrahedral crystal field leads to a lower ligand-field splitting of the 5d levels, and a green emission with moderate wavelength has been obtained.

#### IV. CONCLUSION

Pure AlN:Eu phosphors were successfully synthesized by the gas-reduction-nitridation method. Based on the results of HRTEM, EDS, and EXAFS, Eu occupied a highly distorted Al site coordinated by four nitrogen at about 2.30–2.40 Å, with second nearest neighbors of 12 Al, which could be confirmed by the first-principles calculations. XANES results indicated there were a large amount of Eu<sup>3+</sup> ions accompanying Eu<sup>2+</sup> ions. The Eu<sup>2+</sup> content could be improved by high temperature treatment, improving the green luminescence of the AlN:Eu phosphors.

#### **ACKNOWLEDGMENTS**

This research was supported by the National Natural Science Foundation of China (Grant No. 51072191), Chinese Academy of Sciences under Bairen Program, National Basic Research Program of China (973 Program, 2012CB922004),

Anhui Provincial Natural Science Foundation (11040606M11) and USTC-NSRL Association funding (KY2060140005). The authors thank Shanghai Synchrotron Radiation Facility for providing the XAFS measurements.

- <sup>1</sup>T. Taguchi, IEEJ Trans. Electr. Electron. Eng. **3**, 21 (2008).
- <sup>2</sup>Y. Berencén, J. Carreras, O. Jambois, J. M. Ramírez, J. A. Rodríguez, C. Domínguez, E. Hunt, Charles, and B. Garrido, Opt. Express 19, A234 (2011).
- <sup>3</sup>S. Lee and K. S. Sohn, Opt. Lett. **35**, 1004 (2010).
- <sup>4</sup>R. J. Xie and N. Hirosaki, Sci. Technol. Adv. Mater. **8**, 588 (2007).
- <sup>5</sup>Y. C. Chiu, C. H. Huang, T. J. Lee, W. R. Liu, Y. T. Yeh, S. M. Jang, and R. S. Liu, Opt. Express **19**, A331 (2011).
- <sup>6</sup>T. B. Jackson, A. V. Virkar, K. L. More, R. B. Dinwiddie, and R. A. Cutler, J. Am. Ceram. Soc. **80**, 1421 (1997).
- <sup>7</sup>E. Hagen, Y. Yu, T. Grande, R. Høier, and M. A. Einarsrud, J. Am. Ceram. Soc. 85, 2971 (2002).
- <sup>8</sup>Y. Taniyasu, M. Kasu, and T. Makimoto, Nature 441, 325 (2006).
- <sup>9</sup>V. I. Dimitrova, P. G. Van Patten, H. H. Richardson, and M. E. Kordesch, Appl. Phys. Lett. 77, 478 (2000).
- <sup>10</sup>U. Vetter, J. Zenneck, and H. Hofsass, Appl. Phys. Lett. **83**, 2145 (2003).
- <sup>11</sup>M. L. Caldwell, A. L. Martin, V. I. Dimitrova, P. G. Van Patten, M. E. Kordesch, and H. H Richardson, Appl. Phys. Lett. 78, 1246 (2001).
- <sup>12</sup>H. H. Richardson, P. G. Van Patten, D. R. Richardson, and M. E. Kordesch, Appl. Phys. Lett. 80, 2207 (2002).
- <sup>13</sup>A. Sato, K. Azumada, T. Atsumori, and K. Hara, Appl. Phys. Lett. 87, 021907 (2005).
- <sup>14</sup>M. Peres, A. Cruz, M. J. Soares, A. J. Neves, T. Monteiro, K. Lorenz, and E. Alves, Superlattices Microstruct. 4, 537 (2006).
- <sup>15</sup>N. Hirosaki, R. J. Xie, K. Inoue, T. Sekiguchi, B. Dierre, and K. Tamura, Appl. Phys. Lett. **91**, 061101 (2007).
- <sup>16</sup>B. Dierre, X. L. Yuan, K. Inoue, N. Hirosaki, R. J. Xie, and T. J. Sekiguchi, Am. Ceram. Soc. **92**, 1272 (2009).
- <sup>17</sup>T. Takeda, N. Hirosaki, R. J. Xie, K. Kimoto, and M. J. Saito, J. Mater. Chem. 20, 9948 (2010).
- <sup>18</sup>L. J. Yin, X. Xu, W. Yu, J. G. Yang, L. X. Yang, X. F. Yang, L. Y. Hao, and X. J. Liu, J. Am. Ceram. Soc. 93, 1702 (2010).
- <sup>19</sup>L. J. Yin, W. Yu, X. Xu, L. Y. Hao, and A. Simeon, J. Am. Ceram. Soc. 94, 3842 (2011).

- <sup>20</sup>T. Suehiro, N. Hirosaki, and K. Komeya, Nanotechnology 14, 487 (2003).
  <sup>21</sup>T. Suehiro, N. Hirosaki, R. J. Xie, and M. Mitomo, Chem. Mater. 17, 308
- <sup>22</sup>H. S. Do, S. W. Choi, and S. H. Hong, J. Am. Ceram. Soc. 93, 356 (2010).
- <sup>23</sup>R. J. Xie, N. Hirosaki, K. Sakuma, Y. Yamamoto, and M. Mitomo, Appl. Phys. Lett. **84**, 5404 (2004).
- <sup>24</sup>X. Q. Piao, T. Horikawa, H. Hanzawa, and K. Machida, Appl. Phys. Lett. 88, 161968 (2006).
- <sup>25</sup>Y. F. Wang, X. Xu, L. J. Yin, and L. Y. Hao, J. Am. Ceram. Soc. 93, 1534 (2010).
- <sup>26</sup>U. Vetter, H. Hofsass, and T. Taniguchi, Appl. Phys. Lett. **84**, 4286 (2004).
- <sup>27</sup>T. Miyajima, Y. Kudo, T. Uruga, and K. Hara, Phys. Status Solidi C 3, 1742 (2006).
- <sup>28</sup>C. Ronning, M. Dalmer, M. Uhrmacher, M. Restle, U. Vetter, L. Ziegeler, H. Hofsass, T. Gehrke, K. Jarrendahl, and R. F. Davis, J. Appl. Phys. 87, 2149 (2000).
- <sup>29</sup>J. Mares, R. Baltramiejunas, V. Narkevicius, and J. Vaitkus, Czech. J. Phys., Sect. B 25, 934 (1975).
- <sup>30</sup>H. L. Li, R. J. Xie, N. Hirosaki, T. Takeda, and G. H. Zhou, Int. J. Appl. Ceram. Technol. 6, 459 (2009).
- <sup>31</sup>L. P. Li, Q. Wei, H. J. Li, D. F. Zheng, and Z. W. Su, Z. Phys. B: Condens. Matter 96, 451 (1995).
- <sup>32</sup>J. P. Miao, L. Zhe, L. P. Li, F. L. Ning, Z. G. Liu, X. Q. Sui, Y. Huang, Z. N. Qian, and W. H. Su, J. Alloys Compd. 387, 287 (2005).
- <sup>33</sup>Y. C. Cheng, X. L. Wu, J. Zhu, L. L. Xu, S. H. Li, and P. K. Chu, J. Appl. Phys. **103**, 073707 (2008).
- <sup>34</sup>M. D. Segall, P. J. D. Lindan, M. J. Probert, C. J. Pickard, P. J. Hasnip, S. J. Clark, and M. C. Payne, J. Phys.: Condens. Matter 14, 2717 (2002).
- <sup>35</sup>C. J. Duan, X. J. Wang, and J. T Zhao, J. Appl. Phys. **101**, 023501 (2007).
- <sup>36</sup>J. P. Perdew, K. Burke, and M. Ernzerhof, *Phys. Rev. Lett.* **77**, 3865 (1996).
- <sup>37</sup>D. M. Ceperley and B. Alder, J. Phys. Rev. Lett. **45**, 566 (1980).
- <sup>38</sup>J. P. Perdew and A. Zunger, Phys. Rev. B **23**, 5048 (1981).
- <sup>39</sup>H. Watanabe, H. Yamane, and N. Kijima, J. Solid State Chem. **181**, 1848 (2008)
- <sup>40</sup>K. Shioi, N. Hirosaki, R. J. Xie, T. Takeda, and Y. Q. Li, J. Mater. Sci. 43, 5659 (2008).
- <sup>41</sup>Y. Q. Li, A. C. A. Delsing, R. Metslaar, G. de With, and H. T. Hintzen, J. Alloys Compd. 487, 28 (2009).